Carcinogenesis vol.32 no.6 pp.804–811, 2011
doi:10.1093/carcin/bgr015
Advance Access publication February 2, 2011

Oral administration of penta-*O*-galloyl-β-D-glucose suppresses triple-negative breast cancer xenograft growth and metastasis in strong association with JAK1-STAT3 inhibition

Hyo-Jeong Lee[1], Nam-Jun Seo[1], Soo-Jin Jeong[1], Yongjin Park[1], Deok-Beom Jung[1], Wonil Koh[1], Hyo-Jung Lee[1], Eun-Ok Lee[1], Kwang Seok Ahn[1], Kyoo Seok Ahn[1], Junxuan Lü[2] and Sung-Hoon Kim[1,2,*]

[1]College of Oriental Medicine, Kyung Hee University, Seoul 130-701, Republic of Korea and [2]The Hormel Institute, University of Minnesota, 801 16th Avenue NE, Austin, MN 55912, USA

*To whom correspondence should be addressed. Cancer Preventive Material Development Research Center, College of Oriental Medicine, Kyung Hee University, 1 Hoegi-dong, Dongdaemun-gu, Seoul 131-701, Republic of Korea. Tel: +82 2 961 9233; Fax: +82 2 964 1074;
Email: sungkim7@khu.ac.kr Correspondence may also be addressed to Junxuan Lü. Tel: +1 507 437 9680; Fax: +1 507 437 9606;
Email: jlu@hi.umn.edu

There is an urgent clinical need for chemotherapeutic and chemopreventive drugs for triple-negative breast cancer (TNBCa). Extending on our recent work, we hypothesize that the herbal compound 1,2,3,4,6-penta-*O*-galloyl-beta-D-glucose (PGG) can inhibit the growth and metastasis of TNBCa xenograft and target Janus-activated kinase (JAK)-signal transducer and activator of transcription (STAT) 3-signaling axis. Daily oral gavage of 10 mg PGG/kg body wt decreased MDA-MB-231 xenograft weight by 49.3% ($P < 0.01$) at 40 days postinoculation, whereas weekly intraperitoneal injections of Taxol at the same dosage resulted in a 21.4% reduction ($P > 0.1$). PGG treatment also decreased the incidence of lung metastasis. Immunohistochemical staining detected decreased Ki-67 (proliferation) index and increased terminal deoxynucleotidyl transferase deoxyuridine triphosphate nick end labeling (apoptosis) index in PGG-treated and Taxol-treated xenografts. However, the CD34 (angiogenesis) index was decreased only in PGG-treated xenografts along with decreased phospho-STAT3. In cell culture of MDA-MB-231 cells, PGG decreased pSTAT3 and its downstream target proteins, decreased its upstream kinase pJAK1 and induced the expression of SHP1, a JAK1 upstream tyrosine phosphatase, within as early as 1 h of exposure. The phosphatase inhibitor pervanadate reversed the PGG-induced downregulation of pSTAT3 and caspase activation. Orally administered PGG can inhibit TNBCa growth and metastasis, probably through anti-angiogenesis, antiproliferation and apoptosis induction. Mechanistically, PGG-induced inhibition of JAK1-STAT3 axis may contribute to the observed *in vivo* efficacy and the effects on the cellular processes.

Introduction

Breast cancer (BCa) remains the major cause of cancer-related deaths in women in the USA (1) and worldwide. Approximately 60–70% of BCa cases express estrogen receptor-α (ERα) and/or progesterone receptor, and another ∼20% of cases have amplified human epidermal growth factor receptor (HER)-2 proto-oncogene and express high levels of the HER-2 protein (2). For the majority of organ-confined BCa, which express ERα and progesterone receptor, lumpectomy/mastectomy is often curative. Molecularly targeted therapies that inhibit the estrogen/ERα pathway or that target amplified HER-2 are quite effective in treating the residual diseases in patients whose cancer expresses these targets in an adjuvant therapy context.

Approximately 15–20% of BCa cases are in the category of triple-negative phenotype (2–4), i.e. they lack of ERα and progesterone receptor and do not have amplification of HER-2. These patients have a very poor prognosis because there is no clinically validated molecularly targeted therapy. When surgical and radiation options are no longer applicable to these triple negative breast cancer (TNBCa) patients, treatment with available cytotoxic and genotoxic chemotherapy drugs produces limited efficacy and significant side effects. There remains a strong and urgent need for safer anticancer compounds for the treatment/management of the TNBCa and their metastasis. Novel agents with multiple-targeting ability distinct from the known drugable targets could be useful for circumventing the limitations of current treatment options.

Mammary development occurs through highly coordinated and precise expression/activation of a variety of transcription factors. Inappropriate or constitutive activation of many of these transcription factors is found in BCa and may contribute directly to its pathogenesis (5). Especially, signal transducer and activator of transcription (STAT) proteins have been shown to play an important role in tumor cell survival and proliferation (6). STAT3 is often constitutively active in many human cancer cells and is highly expressed in the TNBCa MDA-MB231 cells (7–9). STAT3 is a latent transcription factor that resides in the cytoplasm. Upon activation by tyrosine phosphorylation, STAT3 dimerizes, translocates to the nucleus and binds to nuclear DNA to modulate transcription of target genes. STAT3 phosphorylation is principally mediated through the activation of non-receptor protein tyrosine kinase family of Janus-activated kinases (JAKs), which include many members JAK1, JAK2, JAK3 and tyrosine kinase 2 (10,11). Additionally, the STAT3 phosphorylation can also be mediated by crosstalk with c-Src kinase (11,12). The major phosphorylation sites in STAT3 include tyrosine and serine residues at positions Tyr^{705} and Ser^{727}, respectively, located in the transactivation domain. The activation of STAT3 results in expression of many target genes required for tumor cell survival (e.g. Bcl-xL, Mcl-1 and survivin), proliferation (e.g. cyclin D1 and c-myc) and angiogenesis [e.g. vascular endothelial growth factor (VEGF)] as well as metastasis (13). Thus, STAT3-signaling pathway has been a favorite therapeutic target for drug development (14,15).

Natural herbal products are potential rich source of chemical inhibitors of STAT3 signaling. 1,2,3,4,6-penta-*O*-galloyl-beta-D-glucose (PGG) (see structure in Figure 1A) is a naturally occurring gallotannin polyphenolic compound in oriental herbs such as *Galla Rhois*, the gallnut of *Rhus chinensis* MILL and the root of peony *Paeonia suffruticosa* Andrews (16). Our collaborative team has recently reported that PGG inhibits both constitutive and cytokine-induced STAT3 phosphorylation in prostate cancer cells *in vitro* and decreased *in vivo* xenograft growth with decreased pSTAT3 in PGG-treated mice (17). The mechanisms of STAT3 inactivation by PGG have not been elucidated.

Earlier work from our group has reported an anti-angiogenic effect of PGG (18) through downregulation of cyclo-oxygenase-2 and VEGF, the latter being a well-recognized target gene of STAT3 (19) and that PGG potently inhibits mouse Lewis lung carcinoma allograft growth in syngenic mice in a dose-dependent manner (18). Recently, PGG has been shown to inhibit PC-3 xenograft growth established in the mouse tibia and to decrease matrix metalloproteinase-9 expression (20), which is a target of STAT3 and is crucial for cancer cell invasion

Abbreviations: BCa, breast cancer; ERK, extracellular signal-related kinase; ERα, estrogen receptor-α; HER, human epidermal growth factor receptor; JAK, Janus-activated kinase; PARP, poly (adenosine diphosphate-ribose) polymerase; PBS, phosphate-buffered saline; PGG, 1,2,3,4,6-penta-O-galloyl-beta-D-glucose; PTP, protein tyrosine phosphatase; STAT, signal transducer and activator of transcription; TNBCa, triple-negative breast cancer; TUNEL, deoxynucleotidyl transferase deoxyuridine triphosphate nick end labeling; VEGF, vascular endothelial growth factor.

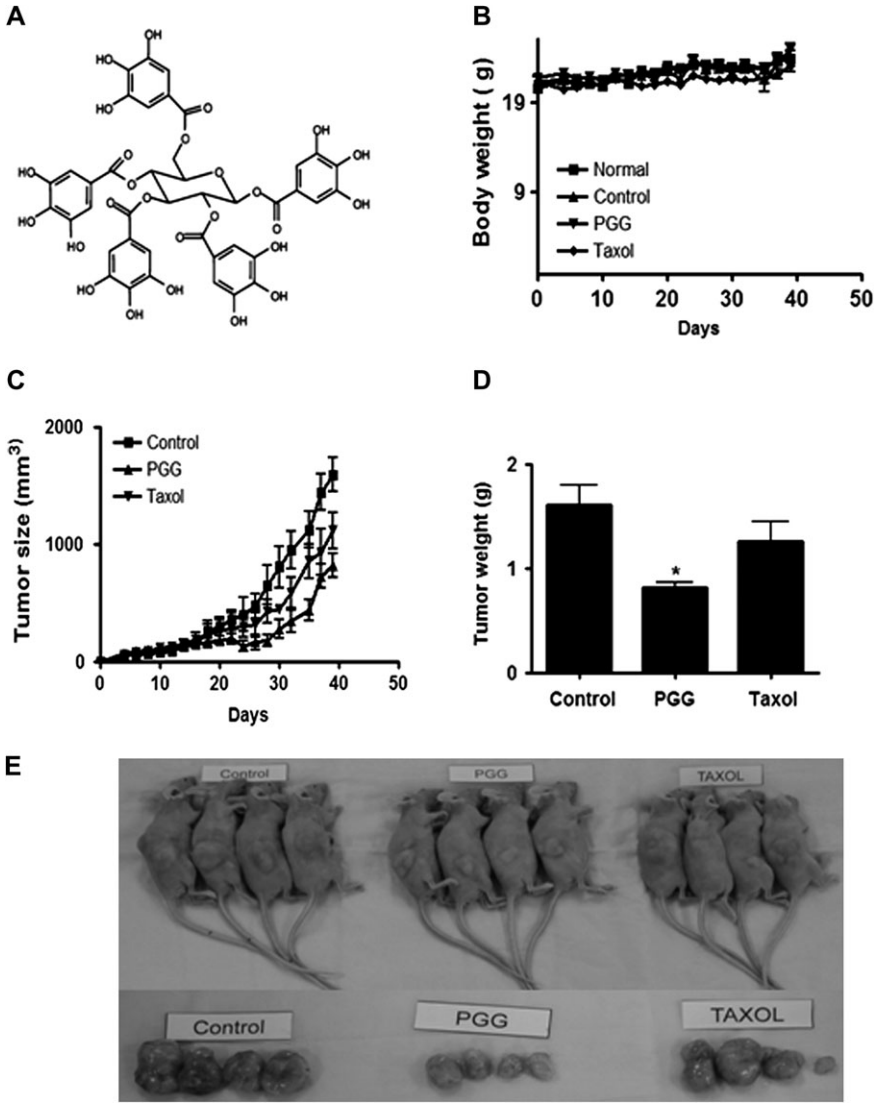

Fig. 1. TNBCa xenograft growth-suppressing activity of PGG in female athymic nude mice. (**A**) Chemical structure of PGG. (**B-E**) Effect of PGG administration by oral gavage on MDA-MB-231 tumor growth. Starting 1 day after cell inoculation, PGG (10 mg/kg body wt) was delivered by feeding needle with 2% Tween-80 as vehicle once daily. Taxol injection (10 mg/kg body wt) was given intraperitoneally once per a week. (B) Body weights of mice. (C) Tumor growth in a time course. (D) Final tumor weight at termination of experiment. Values are means ± standard deviations, n = 8. $^{*}P < 0.05$ compared with control. (E) Photographs of selected tumor bearing mice and their dissected tumors.

and metastasis. Our collaborative team has recently shown, for the first time, an impressive oral efficacy of PGG at 20 mg/kg daily single dosage against xenograft growth established from human MDA-MB-231 TNBCa cells (21).

Here, we confirmed and extended the efficacy evaluation for suppressing not only MDA-MB-231 TNBCa xenograft growth, but also on lung metastasis and established the involvement of suppression of STAT3 signaling *in vivo*. Using cell culture model with this cell line, we aimed at elucidating the molecular mechanisms of PGG-induced STAT3 pathway inactivation.

Materials and methods

Preparation of PGG

PGG used for cell culture studies was isolated from gallnut of *R.chinensis* MILL as described previously (17). The yellowish active compound was identified as PGG by nuclear magnetic resonance and fast atom bombardment mass spectrometry analysis. The purity of PGG was estimated to be >96% by high performance liquid chromatography. The animal study evaluated PGG prepared by methanolysis of tannic acid (purity > 99%) (22).

Cell culture

MDA-MB-231, MDA-MB-435 and MCF-7 BCa cells and MCF-10A normal breast epithelial cells were obtained from Korean cell line bank. MDA-MB-231, MDA-MB-435 and MCF-7 cells were cultured in Dulbecco's modified Eagle medium (Welgene, Daegu, Korea) supplemented with 10% fetal bovine serum (Welgene), penicillin 100 IU/ml and streptomycin 100 μg/ml (Welgene). MCF-10A cells were maintained in Dulbecco's modified Eagle medium/F12 supplemented with 10% fetal bovine serum, epidermal growth factor, insulin, hydrocortisone, cholera toxin, 2 μm L-glutamine and penicillin/streptomycin. The cultures were incubated at 37°C in a humidified incubator with 5% CO_2. The cells were maintained at 70–90% confluence in T-75 flasks.

MDA-MB-231 xenograft model

The animal studies were conducted under guidelines approved by Institutional Animal Care and use Committee, Kyung Hee University [KHUASP(SE)-09-029] and followed a similar protocol as we described previously (21) with minor modifications. Briefly, 1 million MDA-MB-231 cells were mixed with Matrigel (50%, in 100 μl; Becton Dickinson, Bedford, MA) and injected subcutaneously on the right flank of 6-week-old female BALB/c athymic nude mice (NARA Biotech, Seoul, Korea). Three groups of eight mice each were used as follows: 1 day after MDA-MB-231 cell inoculation, a daily gavage treatment of 2% Tween-80 per water was given to the mice in control group,

whereas PGG (10 mg/kg) in dissolved in 2% Tween-80 was orally administered to the mice in PGG group. On the contrary, Taxol (Sigma, St Louis, MO) was intraperitoneally injected into the abdomen of the mice in Taxol group once a week. However, to give equal stresses to three groups, saline was intraperitoneally injected to the mice in control and PGG groups once a week, whereas 2% Tween-80 per water was orally given to the mice in Taxol group except on the injection days of Taxol. The PGG dosage was based on our recently completed study (21) as well as prostate cancer xenograft work (17) and lung cancer allograft work (18). Taxol (10 mg/kg) was dissolved in saline and its purity was ≥97%. Tumors were measured twice per week with a caliper, and tumor volume was calculated as described (23). At end of study, tumors were dissected, weighed and photographed. A piece of each tumor was fixed in 10% phosphate-buffered formalin for histology and immunohistochemistry (IHC). The rest of each tumor was frozen for western blot analyses.

The lungs of the mice were fixed in 10% phosphate-buffered formalin. For detection of pulmonary metastases, the lung tissues were stained for hematoxylin and eosin and Ki-67.

Immunohistochemical staining

For histopathological examination, paraffin sections (4 μm) were stained with hematoxylin and eosin. Immunohistochemical staining for CD34 (Abcam, Boston, MA), deoxynucleotidyl transferase deoxyuridine triphosphate nick end labeling (TUNEL) (Calbiochem, Darmstadt, Germany), pSTAT3 (Cell Signaling Technology, Danvers, MA), Ki-67 (Lab Vision Corporation, Fremont, CA) or VEGF (Santa Cruz Biotechnology, Santa Cruz, CA) was performed using the indirect avidin–biotin-enhanced horseradish peroxidase method. Antigen retrieval was performed after dewaxing and dehydration of the tissue sections by microwave for 10 min in 10 mM citrate buffer. Sections were cooled to room temperature, treated with 3% hydrogen peroxide in methanol for 10 min and blocked with 6% horse serum for 40 min at room temperature. Sections were then incubated with the primary antibody to Ki-67 (diluted 1:200; Lab Vision Corporation), VEGF (diluted 1:200; Santa Cruz Biotechnology) and CD34 (diluted 1:50; Abcam) at 4°C overnight. Sections were washed in phosphate-buffered saline (PBS) and incubated with secondary antibody biotinylated goat anti-rabbit (1:150; Vector laboratories, Burlingame, CA) or biotinylated rabbit anti-rat IgG (1:150; Abcam) for 30 min. After further washes, the antibodies were detected with the Vector ABCcomplex/horseradish peroxidase kit (Vector Laboratories) and color developed with 3,3′-diaminobenzidine tetrahydrochloride.

For semiquantitation, 10 representative ×200 power photomicrographs were taken with a charge coupled device camera, avoiding gross necrotic areas. The positively stained cells per vessels within each photomicrograph were counted. For quantitation, each slide was scanned to get an overall impression of the staining patterns and 10 representative ×200 power photomicrographs were taken with a digital camera, avoiding gross necrotic areas. The positively stained cancer epithelial cells within each photomicrograph were counted. The counting of total cancer cells was aided with the ImagePro+ image-processing program. The TUNEL, STAT3 and Ki-67 indices were based on the counting of ∼7000 total cells per tumor slide. We scored four most vascularized fields of each tumor slide to produce a maximal vessel density count for each tumor.

Cell treatment

MDA-MB-231 cells were seeded in Dulbecco's modified Eagle medium supplemented with 10% fetal bovine serum, 2 μm L-glutamine and penicillin/streptomycin. After 24 h of attachment and growth, cells were treated with varying concentrations of PGG for different duration in serum-free medium. The serum-free medium culture allows us to focus on the autocrine- and paracrine-driven endogenous survival signaling that is characteristic of advanced TNBCa cells including MDA-MB-231 cell line (23,24). Co-treatment with protein tyrosine phosphatase (PTP) inhibitor sodium pervanadate and PGG (10 μM) was carried out for 4 h.

Western blotting

MDA-MB-231 cells exposed to various concentrations of PGG for different duration were harvested and washed with cold PBS. The cells were incubated in lysis buffer [50 mM Tris–HCl (pH 7.4), 150 mM NaCl, 1% Triton X-100, 0.1% sodium dodecyl sulfate and 1 mM ethylenediaminetetraacetic acid] supplemented with protease inhibitors [10 μg/ml leupeptin, 10 μg/ml aprotinin, 10 μg/ml pepstatin A and 1 mM of 4-(2-aminoethyl) benzensulfonyl fluoride] and phosphatase inhibitor (1 mM NaF and 1 mM Na_3VO_4) for 20 min on ice. Lysates were centrifuged at 13 000 r.p.m. for 20 min at 4°C. The supernatant was stored at −20°C. The lysates containing 20 μg of protein were fractionated by sodium dodecyl sulfate–polyacrylamide gel electrophoresis and transferred to a nitrocellulose membrane. The blot was blocked in blocking buffer (5% non-fat dry milk/1% Tween 20 in PBS) for 2 h at room temperature. The blocked membranes were then immunoblotted with primary antibodies (1: 1000 dilution) of phospho-STAT3, STAT3, phospho-JAK1, JAK1, phospho-SRC, SRC, phospho-AKT, AKT, phospho-extracellular signal-related kinase (ERK)1/2, ERK, cleaved poly (adenosine diphosphate-ribose) polymerase (PARP), cleaved caspase3 (Cell Signaling technology, Beverly, MA), Bcl-2, VEGF (Santa Cruz Biotechnology), β-actin (Sigma). The proteins of interest were visualized using horseradish peroxidase-conjugated appropriate secondary antibodies and enhanced chemiluminescence.

RNA isolation and reverse transcription–polymerase chain reaction

Total RNA was prepared using the Trizol reagent (Invitrogen, Carlsbad, CA) according to the manufacturer's instructions and reverse transcribed to complementary DNA using oligo-dT and random primers. The complementary DNA was amplified by polymerase chain reaction using the following specific primers (Cosmo, Seoul, South Korea): *Bcl-2* forward, 5′-TCTTTGAGTTCGGTGGGGTC-3′; reverse, 5′-TGCATATTTGTTTGGGGCAGG-3′; *Cyclin D1* forward, 5′-GCTGGAGCCCGTGAAAAAGA-3v; reverse, 5′-CTCCGCCTCTGGCATTTT G-3′; *Shp-1* forward, 5′-AATGCGTCCCATACTGGCCCG A-3′; reverse, 5′-CCCGCAGTTGGTCACAGAGT-3′; *glyceraldehydes-3-phosphate dehydrogenase (Gapdh)* forward, 5′-TCACCATCTTCCAGGAGCGA-3′; reverse, 5′-CACAATGCCGAAGTGGTCGT-3′. The reaction was performed at 50°C for 30 min, 94°C for 2 min and 30 cycles of 94°C for 15 s, 60°C for 30 s and 72°C for 1 min, with extension at 72°C for 10 min. Polymerase chain reaction products were run on 2% agarose gel and then stained with ethidium bromide. Stained bands were visualized under ultraviolet light and photographed.

Electrophoretic mobility shift assay

The STAT3-DNA binding was analyzed by electrophoretic mobility shift assay using a [γ^{32}P]-labeled high-affinity sis-inducible element (hSIE) probe (5′-CTTCATTTCCCGTAAATCCCTAAAGCT-3′ and 5′-AGCTTTAGGGATTTACGGGAAATGA-3′). Nuclear extracts were prepared from PGG-treated cells for 4 h and incubated with the annealed hSIE duplex probe. The DNA–protein complex formed was separated from free oligonucleotide on 5% native polyacrylamide gels. The dried gels were visualized and the radioactive bands were quantitated with a Storm 820 and Imagequant software (GE Health Care Bio-Sciences, Piscataway, NJ).

siRNA transfection

MDA-MB-231cells at 30–50% confluency were transiently transfected with STAT3-siRNA or control-siRNA (40 nmol/l) (Santa Cruz Biotechnology) for 24 h using INTERFERin™ transfection reagent as shown in manufacturer's protocol. Then, western blotting was performed using STAT3-siRNA or control-siRNA-transfected cells in the presence or absence of PGG.

Statistical analysis

All values represent means ± standard deviations. Statistical differences were tested by analyses of variance of xenograft volume and final weights.

Results

Oral administration of PGG-inhibited MDA-MB231 xenograft growth and lung metastasis in nude mice: efficacy comparison with taxol (paclitaxel)

To confirm the *in vivo* efficacy of PGG and to provide tissues for analyzing biomarkers of efficacy and *in vivo* molecular targets, we included Taxol as a reference drug for efficacy comparison and for distinguishing mechanistic similarities and differences. PGG was given by oral treatment at half the dosage of our reported experiment (21) (i.e. 10 mg/kg body wt), starting 1 day after cancer cell inoculation. Intraperitoneal Taxol injection (10 mg/kg body wt) was given once per week starting 1 day after cancer cell inoculation. As shown in Figure 1C and D, treatment with PGG led to a significant inhibition of tumor growth and decreased the final tumor weight by 49.3% ($P < 0.01$). On the other hand, treatment with Taxol did not result in a statistically significant reduction of the final tumor weight (a numerical 21.4% decrease). The PGG-treated group did not decrease the body weight of the mice (Figure 1B). Taxol treatment slightly suppressed their body weight.

To examine possible impact on metastases, we performed histological evaluation of the lung sections from each mouse (Figure 2A). As shown in Figure 2A, panel a, the metastatic cells were distinguishable on hematoxylin and eosin stained sections from the lung tissue as densely packed irregularly shaped clusters (some marked by arrows).

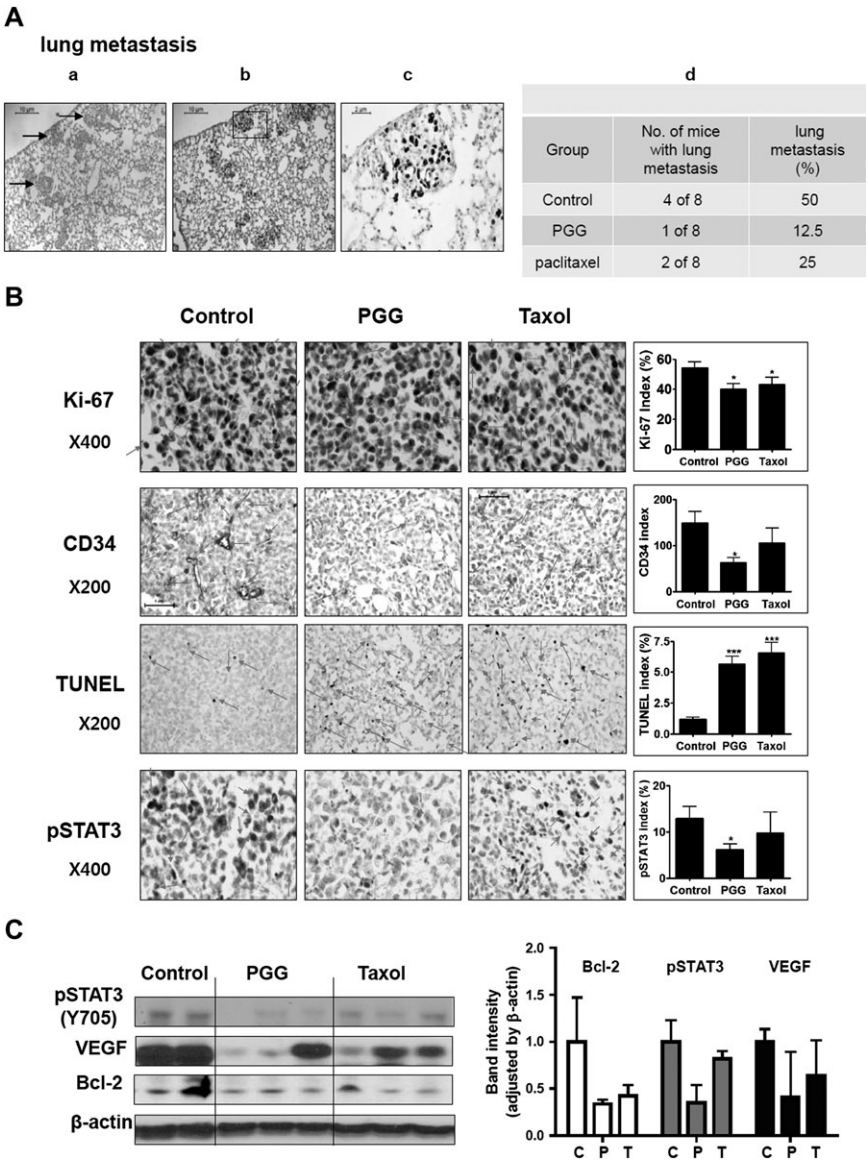

Fig. 2. Effect of PGG on lung metastasis, cancer cell proliferation, apoptosis and angiogenesis in mouse xenograft model. (**A**) Hematoxylin and eosin staining (panel a) and Ki-67 staining (panel b and c) of a lung tissue section from a control mouse showing several deposits of metastatic cancer cells (arrows) in the alveolar septae. Panel d: percentages of lung metastasis in each group. (**B**) Representative examples of immunohistochemical staining for Ki-67, CD34, TUNEL and pSTAT3 in tumor sections. Arrows indicate the immunostained cells for each antibody. Graphs show the Ki-67 index (proliferation), CD34 index (angiogenesis), TUNEL index (apoptosis) and pSTAT3 index in tumor sections. $^{*}P < 0.05$, $^{**}P < 0.01$ and $^{***}P < 0.001$ compared with vehicle treated control mice. (**C**) Western blotting for pSTAT3, VEGF and Bcl-2 of selected tumors. Graphs represent densitometric analysis of the protein expression for pSTAT3, VEGF and Bcl-2.

These cells have much higher Ki-67-labeling index than the lung tissues (Figure 2A, panels b and c). Enumeration of the Ki-67-positive clusters indicated 50% (four of eight mice) incidence of metastasis in the vehicle-treated mice, whereas PGG-treated and Taxol-treated mice showed 12.5% (one of eight mice) and 25% (two of eight mice), respectively (Figure 2A, panel d).

Suppression of pStat3 and VEGF was associated with in vivo apoptosis and anti-angiogenesis in PGG-treated xenograft

Immunohistochemical (IHC) staining of xenograft sections showed significantly decreased proliferation marker Ki-67 positivity in both PGG-treated group and Taxol-treated group (Figure 2B). The vascular endothelial marker protein CD34-positive microvessel counts showed that the microvessel density in the most vascularized area of each tumor was decreased by PGG treatment, but not by Taxol (Figure 2B). Both PGG-treated and Taxol-treated tumors displayed statistically elevated incidence of apoptosis by TUNEL staining (3- to 4-folds). MDA-MB231 is known to express constitutively activated pSTAT3. IHC staining showed intense staining of ∼13% of the nuclei in the control tumors for pSTAT3 (Figure 2B). The pSTAT3-positive fraction was decreased in PGG-treated tumors, whereas Taxol had only minimal effect on pSTAT3 staining (Figure 2B).

Western blot analyses of selected tumor xenograft tissues showed suppression of pSTAT3 and STAT3-regulated proteins VEGF (angiogenesis) and Bcl-2 (anti-apoptosis) in PGG-treated group, whereas the Taxol group was less affected (Figure 2C). Taken together, the biomarker analyses support a strong association of MDA-MB231 xenograft growth inhibition by PGG with suppression of pSTAT3 and its regulated VEGF and Bcl-2 proteins along with decreased *in vivo* angiogenesis and cancer cell proliferation and increased cancer cell apoptosis. The biomarker patterns

also indicated mechanistic distinctions between PGG and Taxol, which targets microtubule assembly and mitotic catastrophe and apoptosis.

PGG inhibited constitutive STAT3 phosphorylation in MDA-MB-231 cells

Next, we focused on using the cell culture model with MDA-MB-231 cells to elucidate mechanisms of action by which PGG-suppressed STAT3 signaling in TNBCa. As expected of constitutively activated STAT3 (9) in MDA-MB231 cells, the basal expression level of pSTAT3 in MDA-MB-231 was markedly higher than non-tumorigenic immortalized MCF-10A cells or estrogen-dependent MCF-7 cells and MDA-MB-435 cells (Figure 3A). PGG exposure in serum-free medium led to a concentration-dependent suppression of constitutive STAT3 activation in MDA-MB-231 cells (Figure 3B) and the inhibitory action was rather rapid (decrease by 70% within 1 h) (Figure 3C). The reduction of pSTAT3 would be predicted to decrease its DNA-binding ability. Indeed, electrophoretic mobility shift assay assay of nuclear extract isolated from the PGG-treated cells showed much decreased binding to labeled STAT3 response element duplex probe (Figure 3D).

As expected from the suppression of pSTAT3 abundance and DNA-binding activity, PGG exposure led to the downregulation of STAT3 target gene products, such as VEGF, Bcl-2 and cyclin D1 (Figure 4A), in general agreement with the *in vivo* findings on these proteins. Measurement of the messenger RNA level of Bcl-2 and cyclin D1 (Figure 4B) showed decreased transcripts of Bcl-2 more than that for cyclin D1, further consistent with an ability of PGG to inhibit STAT3 transcriptional activity.

Knocking down STAT3 increased PGG-induced cell death in MDA-MB-231 cells

Exposure of MDA-MB-231 cells to PGG in serum-free medium induced a time-dependent increase in caspase-3 cleavage activation and the apoptotic cleavage of PARP (Figure 4C). Knocking down of STAT3 level in MDA-MB231 cells increased caspase-mediated apoptosis (Figure 4D, lane 5 versus lane 3). PGG treatment/siRNA-STAT3 led to an additive PARP cleavage when compared with either PGG or si-STAT3 alone, as indicated by the loss of full length PARP (Figure 4D, lane 6 versus lanes 4 and 5).

PGG-induced suppression of STAT3 phosphorylation was reversible in MDA-MB-231 cells

We further examined whether PGG-induced decrease of pSTAT3 was lasting or reversible upon removal of PGG. MDA-MB-231 cells were treated with PGG for 4 h in serum-free medium and then

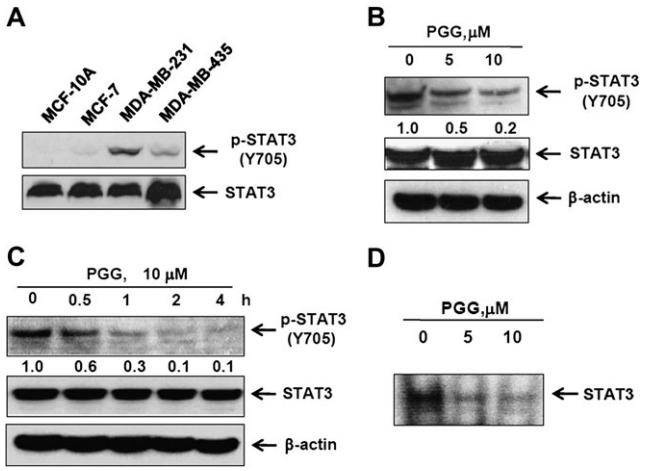

Fig. 3. Inhibitory effects of PGG on constitutive expression and transcriptional activity of STAT3 in MDA-MB-231 cells. (**A**) Cell lysates from non-transformed breast epithelial cell line MCF-10A and BCa cell lines MCF-7, MDA-MB-231 and MDA-MB-435 were prepared and subjected to western blotting to determine the level of phospho-STAT3. (**B** and **C**) MDA-MB-231 cells were treated with the indicated concentration of PGG for 4 h (B) and with 10 μM PGG for the indicated times (C). (**D**) Gel shift mobility assay was performed using nuclear extracts from PGG-treated MDA-MB-231 cells for 4 h to detect STAT3 binding to consensus STAT3 cis element.

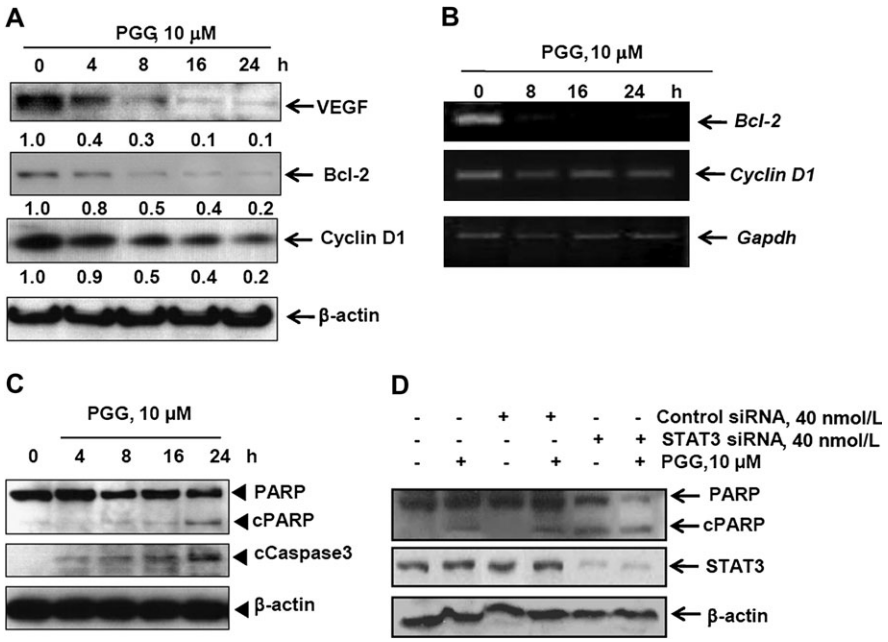

Fig. 4. Effects of PGG on STAT3-target gene products and apoptosis execution molecules in MDA-MB-231 cells. (**A** and **B**) MDA-MB-231 cells were treated with 10 μM PGG for the indicated time. Expressions of VEGF, Bcl-2 and Cyclin D1 at protein and messenger RNA levels were determined by western blotting (A) and reverse transcription–polymerase chain reaction (B), respectively. (**C**) MDA-MB231 cells were treated with 10 μM PGG for the indicated time and western blotting was performed to detect cleavages of PARP and caspase-3. (**D**) MDA-MB-231 cells were treated with 10 μM PGG and/or control RNA or STAT3 siRNA (40 nmol/l) for 24 h and western blotting was performed to detect PARP cleavage.

the cells were washed twice with PBS to remove PGG. The cells were then cultured in fresh serum-free medium for different durations, and the level of pSTAT3 was measured. The removal of PGG resulted in a gradual recovery of pSTAT3, starting at 4 h (Figure 5A) without changing STAT3 protein level.

PTP inhibitor blocked PGG-induced STAT3 dephosphorylation

PTPs have been implicated in pSTAT3 deactivation (25). Therefore, we examined whether PGG-induced inhibition of STAT3 tyrosine phosphorylation could be due to the activation of a PTP. Treatment of MDA-MB-231 cells with the broad acting tyrosine phosphatase inhibitor sodium pervanadate reversed the PGG-induced inhibition of STAT3 phosphorylation in a concentration-dependent manner (Figure 5B). Furthermore, pervanadate attenuated the PGG-induced caspase cleavage of PARP (Figure 5C). This suggested that the PTPs were involved in PGG-induced inhibition of STAT3 phosphorylation and in signaling to apoptosis.

PGG-induced PTP SHP-1

The PTP member SHP-1 is a known upstream regulator of STAT3 activation through dephosphorylation of its upstream activator kinase JAK (26). Western blotting detected a time-dependent rapid induction of SHP-1 protein (Figure 5D), which was accompanied by increased messenger RNA level detectable by reverse transcription–polymerase chain reaction (Figure 5E) in a lockstep manner.

PGG suppressed constitutive activation of JAK1and Src

Because STAT3 is activated by soluble tyrosine kinases of the Janus family and JAK1 is one of the main kinases [11], we examined the effects of PGG on JAK1 phosphorylation. The results showed that PGG treatment led to an inhibition of constitutive activation of JAK1 in a concentration- and time-dependent manner (Figure 6A and B). It is noteworthy that JAK1 deactivation by PGG treatment was rapid in temporal synchrony with pSTAT3 dephosphorylation. Although the Src oncoprotein kinase also activates STAT3 (11,12), PGG treatment decreased pSrc in a much slower temporal course than pJAK1.

Differential effects of PGG on other protein kinases in MDA-MB-231 cells

Interestingly, PGG treatment did not decrease AKT phosphorylation, consistent with our findings in prostate cancer cells (26), but decreased the phosphorylated ERK, especially ERK2 and the stress-activated c-Jun N-terminal kinase 1/2 rapidly (Figure 6C and D).

Discussion

Our *in vivo* data demonstrate a growth inhibitory efficacy of orally administered PGG against MDA-MB231 TNBCa xenograft and lung metastasis (Figure 1). The fact that PGG is orally available and therefore can be self administered by patients will have a major impact on reducing the health care delivery cost, compared with injection-only

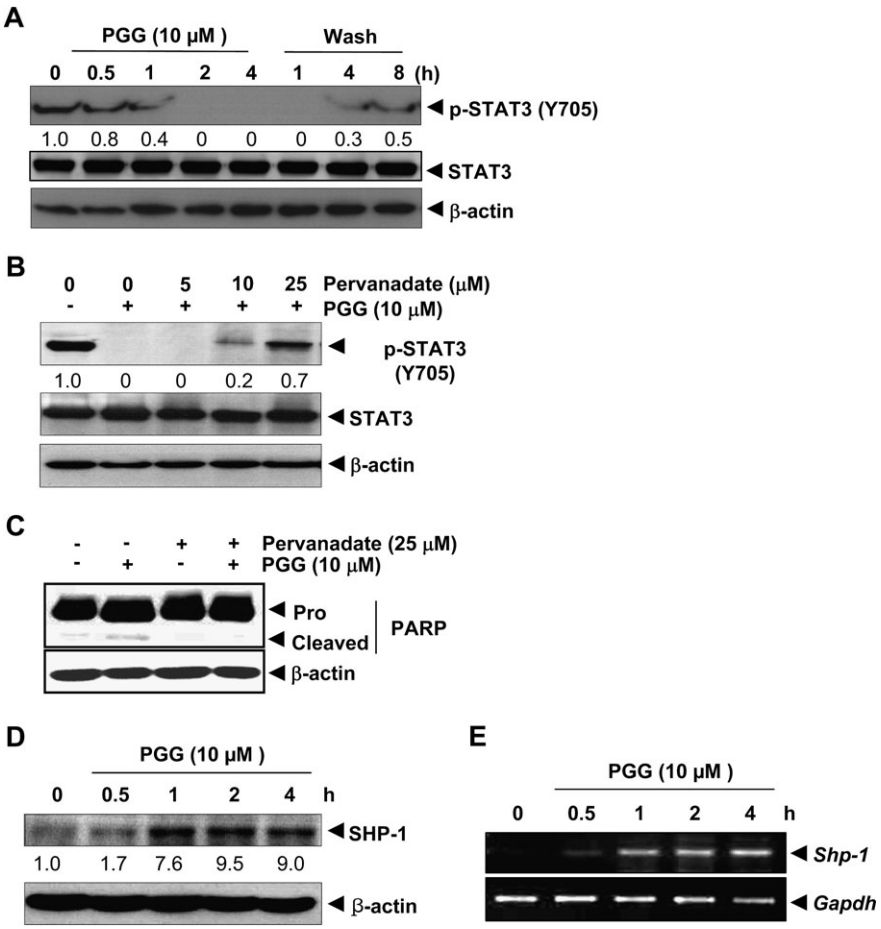

Fig. 5. Reversibility of PGG-induced inhibition of STAT3 and PGG-induced SHP-1 expression in MDA-MB-231 cells. (**A**) MDA-MB-231 cells were treated with 10 μM PGG for up to 4 h and washed with PBS twice to remove PGG before refeeding in fresh medium. Whole cell extract was prepared for western blotting. (**B** and **C**) MDA-MB-231 cells were treated with the indicated concentrations of pervanadate and 10 μM PGG for 4 h for cellular extracts. For western blotting, 20 μg of whole cell extracts were immunobloted for pSTAT3 and total STAT3. (**D** and **E**) Expression of SHP-1 at protein and messenger RNA levels was determined by western blotting (D) and reverse transcription–polymerase chain reaction (E), respectively.

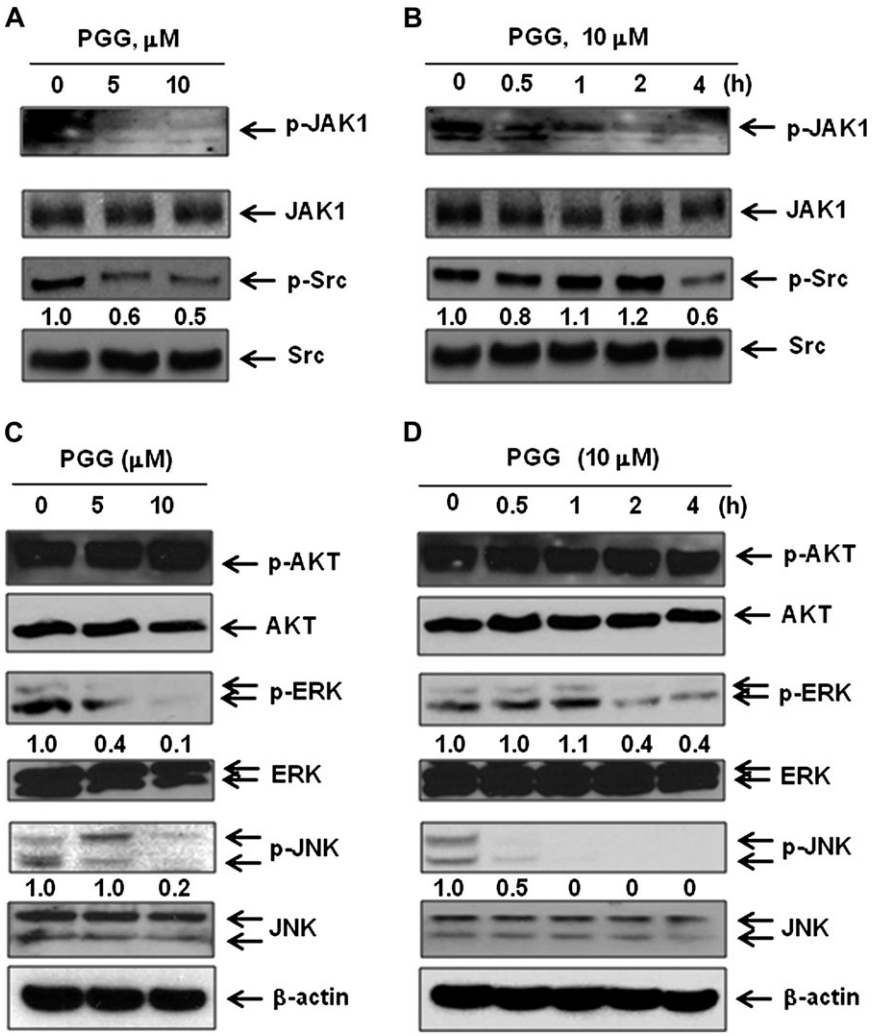

Fig. 6. Inhibitory effects of PGG on JAK1, Src, ERK and c-Jun N-terminal kinase 1/2 in MDA-MB-231 cells. (**A–D**) MDA-MB-231 cells were treated with the indicated concentration of PGG for 4 h (A and C) and with 10 μM PGG for the indicated times (B and D). Western blotting was performed to determine levels of phospho-JAK1 and Src (A and B) and phospho-AKT, ERK and c-Jun N-terminal kinase (C and D).

drugs (such as Taxol) that have to be given by health care professionals. In addition to the suppression efficacy against the growth of inoculated primary cancer, PGG also decreased the incidence of metastasis to the lung (Figure 2A). The STAT3 pathway has been strongly linked to cancer angiogenesis, inflammation and metastasis (13,19,27). The observed suppression by PGG treatment on pSTAT3 in tumor tissues (detected by IHC and western blotting) and its target proteins such as VEGF and Bcl-2, but not by Taxol treatment, suggest a potential *in vivo* molecular target pathway of PGG for contributing to/mediating antiproliferation, anti-angiogenesis, apoptosis and anti-metastasis (Figure 2).

Our investigation with the cell culture model (Figures 3–6) confirmed our early report of inhibition of STAT3 signaling by PGG in prostate cancer cells (17). We showed not only reduction in pSTAT3 and its DNA-binding activity in MDA-MB231 cells *in vitro* (detected by western blotting and electrophoretic mobility shift assay) (Figure 3), but also downregulation of many of its important targets involved in angiogenesis, cell survival and proliferation (Figure 4). Furthermore, our data produced additional insights into how PGG inactivates the STAT3 pathway. The simultaneous downregulation of pJAK1 with pSTAT3 suggested targeting this upstream activator of STAT3 by PGG (Figure 6). The ability of the PTP inhibitor pervanadate to reverse pSTAT3 dephosphorylation strongly suggested the induction of one or more PTPs by PGG. Our results (Figure 5D and E) suggested SHP-1 as one such PTP that could be rapidly induced by PGG to deactivate pJAK and the pSTAT3-signaling axis.

In summary, our *in vivo* data support oral efficacy of PGG against the growth and metastasis of a triple-negative BCa model, rivaling that of Taxol and with mechanistic differences from this first line chemotherapy drug. The inhibition of the activated STAT3 pathway contributed, at least in part, to the tumor growth efficacy and anti-metastasis through antiproliferative, anti-angiogenic and apoptosis induction.

Funding

Korean Ministry of Education, Science and Technology (Medical Research Center grant No. 2010-0063466); Hormel Foundation and National Institute of Health (CA136953).

Conflict of Interest Statement: None declared.

References

1. Jemal,A. *et al*. (2008) Cancer statistics, 2008. *CA Cancer J. Clin.*, **58**, 71–96.

2. Cleator,S. *et al*. (2007) Triple-negative breast cancer: therapeutic options. *Lancet Oncol.*, **8**, 235–244.
3. Irvin,W.J.Jr. *et al*. (2008) What is triple-negative breast cancer? *Eur. J. Cancer.*, **44**, 2799–2805.
4. Rakha,E.A. *et al*. (2009) Triple-negative breast cancer: distinguishing between basal and nonbasal subtypes. *Clin. Cancer Res.*, **15**, 2302–2310.
5. Visvader,J.E. *et al*. (2003) Transcriptional regulators in mammary gland development and cancer. *Int. J. Biochem. Cell Biol.*, **35**, 1034–1051.
6. Darnell,J.E.Jr. (2002) Transcription factors as targets for cancer therapy. *Nat. Rev. Cancer.*, **2**, 740–749.
7. Bharti,A.C. *et al*. (2003) Curcumin (diferuloylmethane) inhibits constitutive and IL-6-inducible STAT3 phosphorylation in human multiple myeloma cells. *J. Immunol.*, **171**, 3863–3871.
8. Buettner,R. *et al*. (2002) Activated STAT signaling in human tumors provides novel molecular targets for therapeutic intervention. *Clin. Cancer Res.*, **8**, 945–954.
9. Berishaj,M. *et al*. (2007) Stat3 is tyrosine-phosphorylated through the interleukin-6/glycoprotein 130/Janus kinase pathway in breast cancer. *Breast Cancer Res.*, **9**, R32.
10. Ihle,J.N. (1996) STATs: signal transducers and activators of transcription. *Cell*, **84**, 331–334.
11. Ren,Z. *et al*. (2002) ErbB-2 activates Stat3 alpha in a Src- and JAK2-dependent manner. *J. Biol. Chem.*, **277**, 38486–38493.
12. Schreiner,S.J. *et al*. (2002) Activation of STAT3 by the Src family kinase Hck requires a functional SH3 domain. *J. Biol. Chem.*, **277**, 45680–45687.
13. Devarajan,E. *et al*. (2009) STAT3 as a central regulator of tumor metastases. *Curr. Mol. Med.*, **9**, 626–633.
14. Yu,H. *et al*. (2004) The STATs of cancer–new molecular targets come of age. *Nat. Rev. Cancer.*, **4**, 97–105.
15. Aggarwal,B.B. *et al*. (2006) Targeting signal-transducer-and-activator-of-transcription-3 for prevention and therapy of cancer: modern target but ancient solution. *Ann. N. Y. Acad. Sci.*, **1091**, 151–169.
16. Zhang,J. *et al*. (2009) Anti-cancer, anti-diabetic and other pharmacologic and biological activities of penta-galloyl-glucose. *Pharm. Res.*, **26**, 2066–2080.
17. Hu,H. *et al*. (2008) Penta-1,2,3,4,6-O-galloyl-beta-D-glucose induces p53 and inhibits STAT3 in prostate cancer cells *in vitro* and suppresses prostate xenograft tumor growth *in vivo*. *Mol. Cancer Ther.*, **7**, 2681–2691.
18. Huh,J.E. *et al*. (2005) Penta-O-galloyl-beta-D-glucose suppresses tumor growth via inhibition of angiogenesis and stimulation of apoptosis: roles of cyclooxygenase-2 and mitogen-activated protein kinase pathways. *Carcinogenesis*, **26**, 1436–1445.
19. Niu,G. *et al*. (2002) Constitutive Stat3 activity up-regulates VEGF expression and tumor angiogenesis. *Oncogene*, **21**, 2000–2008.
20. Kuo,P.T. *et al*. (2009) Penta-O-galloyl-beta-D-glucose suppresses prostate cancer bone metastasis by transcriptionally repressing EGF-induced MMP-9 expression. *J. Agric. Food Chem.*, **57**, 3331–3339.
21. Chai,Y. *et al*. (2010) Penta-O-galloyl-beta-D-glucose induces G1 arrest and DNA replicative S-phase arrest independently of cyclin-dependent kinase inhibitor 1A, P27 cyclin-dependent kinase inhibitor 1B and P53 in human breast cancer cells and is orally active against triple negative xenograft growth. *Breast Cancer Res.*, **12**, R67.
22. Li,L. *et al*. (2010) Preparation of penta-O-galloyl-beta-d-glucose from tannic acid and plasma pharmacokinetic analyses by liquid-liquid extraction and reverse-phase HPLC. *J. Pharm. Biomed. Anal.*, **54**, 545–550.
23. Li,L. *et al*. (2002) Autocrine-mediated activation of STAT3 correlates with cell proliferation in breast carcinoma lines. *J. Biol. Chem.*, **277**, 17397–17405.
24. Lieblein,J.C. *et al*. (2008) STAT3 can be activated through paracrine signaling in breast epithelial cells. *BMC Cancer*, **8**, 302.
25. Bittorf,T. *et al*. (1999) SHP1 protein tyrosine phosphatase negatively modulates erythroid differentiation and suppression of apoptosis in J2E erythroleukemic cells. *Biol. Chem.*, **380**, 1201–1209.
26. Hu,H. *et al*. (2009) Pentagalloylglucose induces autophagy and caspase-independent programmed deaths in human PC-3 and mouse TRAMP-C2 prostate cancer cells. *Mol. Cancer Ther.*, **8**, 2833–2843.
27. Yu,H. *et al*. (2009) STATs in cancer inflammation and immunity: a leading role for STAT3. *Nat. Rev. Cancer.*, **9**, 798–809.

Received November 26, 2010; revised January 4, 2011; accepted January 15, 2011